A broadband pulsed radio frequency electron paramagnetic resonance spectrometer for biological applications

Ramachandran Murugesan,[a] Mobae Afeworki, John A. Cook, Nallathamby Devasahayam, Rolf Tschudin, James B. Mitchell, Sankaran Subramanian, and Murali C. Krishna[b]
Radiation Biology Branch, Division of Clinical Sciences, National Cancer Institute, NIH, Bethesda, Maryland 20892

(Received 10 October 1997; accepted for publication 29 January 1998)

A time-domain radio frequency (rf) electron paramagnetic resonance (EPR) spectrometer/imager (EPRI) capable of detecting and imaging free radicals in biological objects is described. The magnetic field was 10 mT which corresponds to a resonance frequency of 300 MHz for paramagnetic species. Short pulses of 20–70 ns from the signal generator, with rise times of less than 4 ns, were generated using high speed gates, which after amplification to 283 Vpp, were deposited into a resonator containing the object of interest. Cylindrical resonators containing parallel loops at uniform spacing were used for imaging experiments. The resonators were maintained at the resonant frequency by tuning and matching capacitors. A parallel resistor and overcoupled circuit was used to achieve Q values in the range 20–30. The transmit and receive arms were isolated using a transmit/receive diplexer. The dead time following the trailing edge of the pulse was about 450 ns. The first stage of the receive arm contained a low noise, high gain and fast recovery amplifier, suitable for detection of spin probes with spin-spin relaxation times (T_2) in the order of μs. Detection of the induction signal was carried out by mixing the signals in the receiver arm centered around 300 MHz with a local oscillator at a frequency of 350 MHz. The amplified signals were digitized and summed using a 1 GHz digitizer/summer to recover the signals and enhance the signal-to-noise ratio (SNR). The time-domain signals were transformed into frequency-domain spectra, using Fourier transformation (FT). With the resonators used, objects of size up to 5 cm^3 could be studied in imaging experiments. Spatial encoding of the spins was accomplished by volume excitation of the sample in the presence of static field gradients in the range of 1.0–1.5 G/cm. The spin densities were produced in the form of plane integrals and images were reconstructed using standard back-projection methods. The image resolution of the phantom objects containing the spin probe surrounded by lossy biologic medium was better than 0.2 mm with the gradients used. To examine larger objects at local sites, surface coils were used to detect and image spin probes successfully. The results from this study indicate the potential of rf FT EPR for *in vivo* applications. In particular, rf FT EPR may provide a means to obtain physiologic information such as tissue oxygenation and redox status.
[S0034-6748(98)05304-0]

I. INTRODUCTION

Free radicals are recognized to either participate in or actually cause many chronic as well as acute pathological conditions. Therefore, techniques for *in vivo* detection of free radicals are receiving increasing attention. Electron paramagnetic resonance (EPR) spectroscopy is one of very few techniques used to directly detect, characterize, and quantitate paramagnetic species such as transition metal complexes or free radicals. In the radio frequency (rf) range, the incident electromagnetic radiation (EMR) adequately penetrates the object under study with minimal nonresonant absorption. Therefore at these frequencies, EPRI holds the potential to detect and image free radicals noninvasively. Based on considerations of the penetration of EMR in biological objects,[1–4] EPR spectrometers have to be implemented in the radio frequency range for *in vivo* studies.

With the development of loop gap resonators, based on lumped circuit design that provide optimal E- and B_1-field profiles while minimizing the nonresonant absorption,[5] *in vivo* EPR studies on lossy biologic samples were shown to be feasible using continuous wave (cw) techniques at rf and microwave frequencies.[6–12] Most of the spectrometers described for *in vivo* applications acquire data by operating in the ''frequency domain'' of data acquisition, wherein at a fixed frequency the magnetic field is swept to obtain an absorption spectrum. Such techniques, called continuous wave (cw) techniques do not impose any restriction on the spectral or line width of the species under examination. However, imaging studies using cw techniques are compromised because the spectral acquisition times (500 ms–10 s) are in the same range as or longer than those of physiological motions such as heart beat, peristalsis, respiration, etc. Additionally,

[a]Present address: School of Chemistry, Madurai Kamaraj University, Madurai, India.
[b]Author to whom correspondence should be addressed; electronic address: murali@helix.nih.gov

in cw EPR, artifacts associated with sweep rates, magnetic field modulation, and power saturation can distort the spectra.

To enhance the sensitivity of detection, frequency domain data acquisition techniques have been replaced in nuclear magnetic resonance (NMR) by time-domain data acquisition coupled with Fourier transformation (FT), exploiting the Fellgett multichannel advantage.[13] Such techniques provide distinct advantages in terms of enhanced signal-to-noise ratio (SNR), particularly in ^{1}H and ^{13}C NMR, where the spectral line widths are in the Hz–kHz range corresponding to spin-spin relaxation times in the order of s–ms. However, such time-domain methods were found to be difficult to implement in EPR because of the naturally broad resonances, with spin-spin relaxation times in the order of μs–ns. In addition, the spectral windows required to study organic free radicals are in the range of tens of MHz, requiring intense pulses with widths of a few nanoseconds and very low Q values for the resonators to accommodate the spectral bandwidth. In spite of such difficulties, pulsed EPR spectrometers have been implemented to operate at frequencies such as L, S, X, and W band for spectroscopic and imaging experiments.[14–19] However, the implementation of pulsed EPR methods at radiofrequencies (rf) for *in vivo* applications is further complicated because of the following reasons:

(1) Narrow pulses are required to have broad spectral coverage. The narrow pulses should encompass several cycles of the incident frequency of the EMR to have reasonable selectivity in excitation.

(2) Dead times associated with resonator ringing are inversely related to the frequency of operation. The dead time T_d is related to the time constant for the resonator dead time,[20] and is expressed as

$$T_d = n\tau = n(Q/2\pi\nu),$$

where τ is the time constant of the resonator ringing, Q is the quality factor of the resonator, and ν is the frequency of operation, and n is the number of ringing time constants for the receiver to arrive at thermal noise level. Useful data in the time domain can be collected only after the input pulse power has decayed to the detector noise level. At rf (200–300 MHz) with 200 W input power, n would be approximately 20–25 for a Q in the range of 25–30. Thus, with weak signals, useful spectral data can be collected only after a dead time ranging from 300 to 600 ns following the trailing edge of the pulse.

(3) Spin-spin relaxation times of most spin probes, such as nitroxides, are in the nanosecond time range; therefore, the signal in the time domain would not be expected to persist beyond the resonator dead time.

However, the feasibility of detecting resonance signals at rf (300 MHz) with a time-domain data acquisition has been shown for spin probes having single line EPR spectra with narrow linewidths using small volume resonators.[21,22] Likewise, in the presence of static gradients, the feasibility of *in vivo* spatial imaging has also been demonstrated.[21,23] As a result of newly developed biologically compatible spin probes that have single narrow lines, time-domain EPR for *in vivo* applications is a technique with potential for obtaining physiological and anatomical information.[23] In the present report, a broadband time-domain EPR spectrometer suitable for *in vivo* applications is described. This spectrometer has been configured to utilize signal processing strategies reported earlier[22] to avoid quadrature detection while retaining the information on the sign of the signals. Details of the spectrometer and some results from spectroscopic and imaging experiments utilizing a resonator of 25 mm diameter and 25 mm height on phantom objects are described.

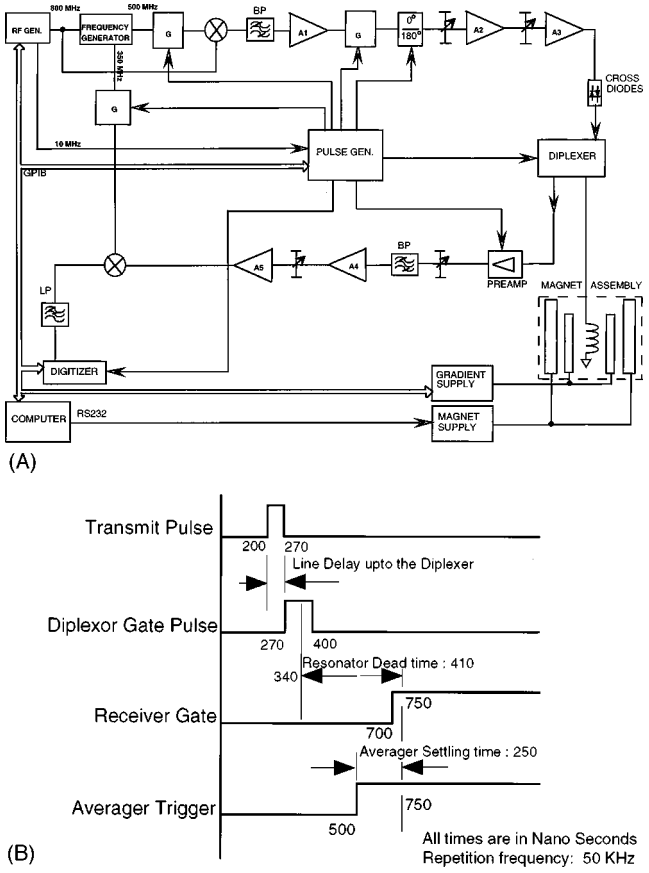

FIG. 1. (A) Block diagram of the time-domain rf FT EPR spectrometer/imager. (B) Typical timing diagram of the spectrometer.

II. INSTRUMENTATION

A. Spectrometer

Figure 1(A) shows a block diagram of the time-domain rf EPR spectrometer operating typically at 300 MHz. All the timing signals were generated by a set of four daisy-chained digital delay generators (DG 535, Stanford Research Systems, Sunnyvale, CA). To reduce jitter, the master clock signal of 10 MHz from the signal generator was used as an external clock to the four delay generators and as an external trigger input to the first delay generator. The other three delay generators were synchronized with the first delay generator. Figure 1(B) provides a typical timing sequence of a single pulse experiment.

B. Transmitter arm

The rf signal (300 MHz) and the local oscillator frequency of 350 MHz were synthesized from a single signal

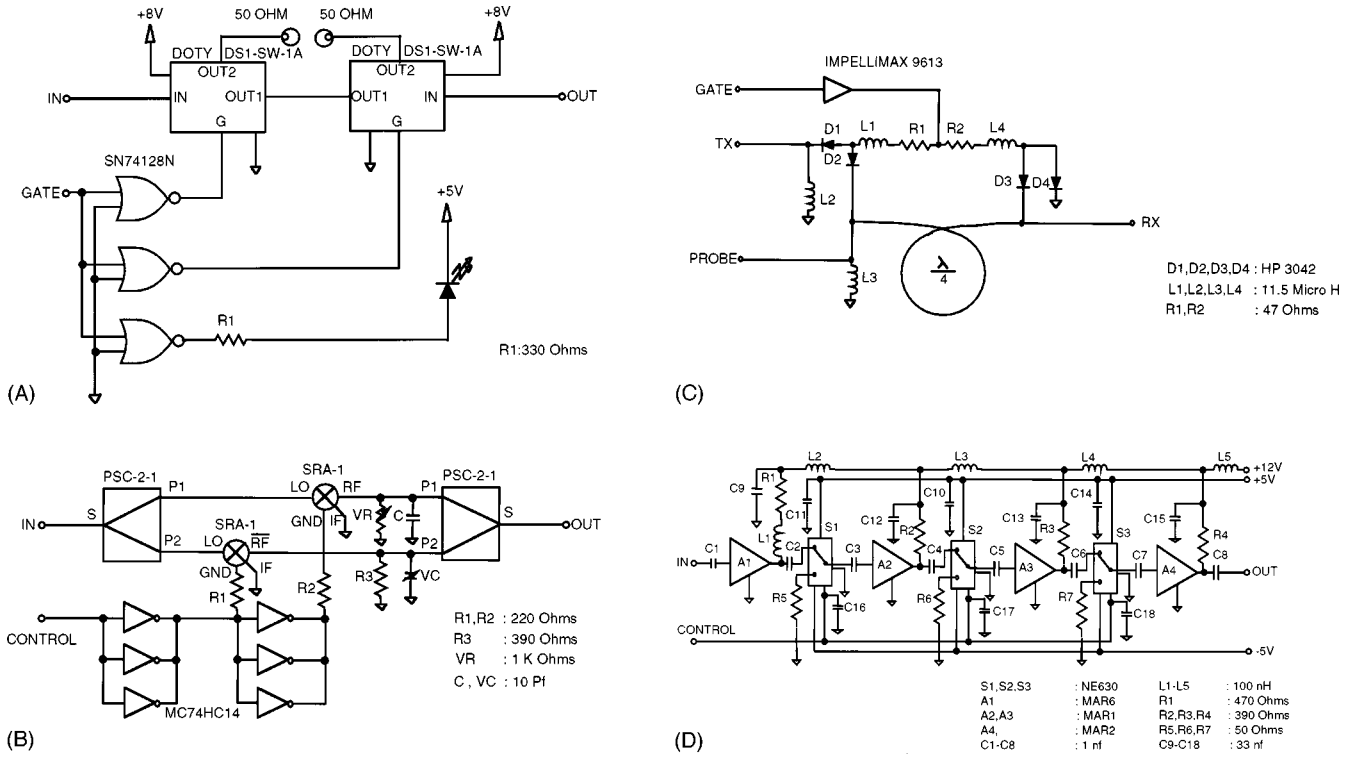

FIG. 2. (A) High speed rf gate; (B) 0°/180° phase switch; (C) transmit/receive diplexer; and (D) four-stage gated amplifier.

generator (HP 8644, Hewlett Packard, Palo Alto, CA) set at 800 MHz, and using frequency dividers, bandpass filters, and rf amplifiers. Appropriate gating of the signals which are input to mixers is done to avoid undesired feedthrough during FID acquisition. The 300 MHz signal was amplified by A1 (25 dB gain, homebuilt Motorola MHW590) and the amplified signal was pulse modulated using high speed rf gates which consist of two GaAs SPDT switches (SW-1, Doty Scientific Inc., Columbia, SC) as shown in Fig. 2(A). The switches were connected back-to-back to achieve an isolation of >80 dB. The pulses generated by the gates had rise and fall times of less than 4 ns. The pulse modulated 300 MHz output was fed through a 0°/180° phase switch [Fig. 2(B)] to an intermediate rf power amplifier, A2 (gain 25 dB, homebuilt with Motorola MHW 590). After attenuating to the required power level, the pulses were equally divided using a power splitter (ZSC-2-1W, Mini-Circuits, Brooklyn, NY). The divided pulses were amplified using two high power rf amplifiers, A3 (100 W, 5100 L, ENI, Rochester, NY). The outputs from each amplifier were combined using a power combiner (ANTPD33, Telewave Inc., Mountain View, CA) and fed to the resonator through a transmit/receive switch (diplexer) [Fig. 2(C)]. Amplifier noise was reduced by incorporating several pairs of crossed diodes. Manually adjustable attenuators were included at various stages to set the appropriate voltage levels to avoid overloads.

C. Diplexer

A single coil probe was used for the experiments with a diplexer. The diplexer used in this study was of a standard $\lambda/4$ configuration with a series pin-diode switch assembly (D1, D2) in the transmitter path and a shunt pin-diode switch assembly (D3, D4) in the receiver path [Fig. 2(C)]. These diodes were connected in a back-to-back configuration to minimize the transients in the rf paths, which were held to ground by rf chokes (L2, L3). The arrangement provided high speed switching (about 5 ns) necessary for time-domain rf FT EPR experiments. Receiver isolation during transmit mode was 25 dB with a transmit insertion loss of 2 dB. The insertion loss during receive mode was 0.5 dB. Circulators were also evaluated for the feasibility of adequately isolating the transmit and receive modes with comparable results to those obtained with the diplexer.

D. Resonators

Resonators were designed for the rf FT EPR experiments to obtain: (a) optimal, homogeneous B_1 field within the resonator for a given transmit power; (b) resonator bandwidth to encompass a spectral bandwidth of 12 MHz; and (c) minimize resonator ringing and consequently shorten the dead time. Factors (b) and (c) limit the Q values at 300 MHz resonant frequency to 25–30. An overcoupled resonator which had a diameter of 25 mm and a height of 25 mm containing 11 parallel loops 2.5 mm apart, was used for detection [Fig. 3(A)]. These dimensions were adequate to accommodate an experimental animal, such as a mouse, for imaging studies. The loaded Q of the coil was maintained at 25. To obtain volume resonators, loops of conducting material spaced at equal intervals along the cylindrical axis, were connected in parallel. Q reduction in these resonators was achieved by overcoupling. In addition, a resistance in parallel (3.3 kΩ) is also used to minimize the dead time and also help reach the desired spectral bandwidth. The inclusion of this high value resistor did not cause significant loss in

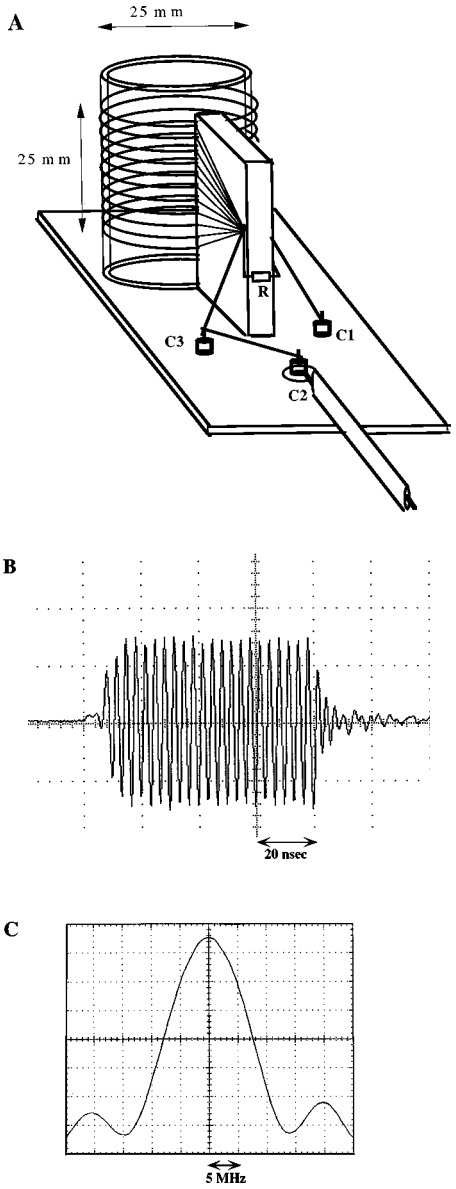

FIG. 3. (A) A schematic of the parallel coil resonator. The eleven turns of identical segment length connected in parallel, tuned, and matched by overcoupling with an additional 3.3 kΩ resistor, had a Q of 25. The inner diameter and the length of the cylindrical resonator were both 25 mm. (B) Gated pulses of 70 and 30 ns width and (C) the corresponding power spectra showing the bandwidth that can be covered with the 200 W amplifier.

power. Pulses down to 30 ns gave a power spectrum almost close to the theoretical expectation. The rise and fall times of the pulses were less than 3 ns. Pulses of 70 ns duration (283 Vpp), were used for excitation [Fig. 3(B)]. The spectral bandwidth afforded by such pulses was at least 12 MHz [Fig. 3(C)]. Surface coil resonators were designed by connecting loops of the required diameter to a $\lambda/2$ length semirigid coaxial line to allow for separation between the coil, and the tuning and matching capacitors.

E. Signal amplification

The first stage amplifier in the detector arm is critical in any time-domain magnetic resonance experiment. In EPR, the problems are compounded because amplifiers must recover quickly and must have high gain. A fast recovery, high gain amplifier in four stages was incorporated in the first stage of the receive arm [Fig. 2(D)]. The four-stage amplifier composed of MAR series amplifiers (Mini-Circuits, Brooklyn, NY) contains BiC MOS SPDT switches (NE630/Philips Semiconductors, Sunnyvale, CA) between the stages, to prevent each amplification stage from changing its bias condition because of overload, and so assure rapid recovery. At each amplification stage, the signal is inverted in phase to minimize the transients produced by successive stages. Linear amplification with a gain of 41 dB is obtained 40 ns after the switches are on. The amplifier was centered around 300 MHz with a bandwidth of 100 MHz and a noise figure of 3 dB. The gating signal was provided by one of the delay generators.

After the first stage amplification, the signal was filtered with a 300 MHz center frequency bandpass filter having a bandwidth of 42 MHz (TTE/07766-KC6-300M-14P-50-6140, TTE Inc., Los Angeles, CA) and subsequently amplified by a low-noise amplifier, A4 (Miteq 2A 150, 25 dB, Hauppauge, NY) and a rf amplifier, A5 (gain 25 dB, Model MHW590, Motorola). Adjustable attenuators were used to set the appropriate levels.

F. Single channel/quadrature operation

The induction signals from the receiver arm were mixed with a local oscillator (350 MHz) eliminating the need for quadrature detection while still retaining the information of the sign of the signals. The FID with the intermediate 50 MHz signal (IF) was isolated using a low pass filter and utilized for digitization and recovering the FID. A mixer (Mini-Circuits, ZP 10514) was used for phase-sensitive detection.

G. Digitizer/summer

The FIDs were digitized and summed by a custom-built Analytek/Tektronix 2000RV2 digitizer/summer (Tektronix, Sunnyvale, CA). The digitizer/summer consists of four interleaved flash analog-to-digital converters. Each unit has a digitizing speed of 500 MS/s and a minimum retrigger period of 4.2 μs. The sampling unit can provide 1 GS/s in single- or double-channel modes at 8-bit vertical resolution. The summer captures the digitized wave forms from the sampler and adds them into a 32-bit buffer. A mode is provided which allows summing and digitizing operations to overlap so that 4 k wave forms can be summed at a rate of 238 000 per second. However, in view of the cycle time (50 kHz) to take care of the relaxation, the full capability of the digitizer/summer is seldom used. The summed signal was downloaded to a host computer for further data processing.

H. Image reconstruction

The FIDs collected were treated with a digital Butterworth bandpass filter of appropriate window of approximately ± 10 MHz from the carrier. These were further processed with resolution/sensitivity enhancing filters as needed.[24] Finally, the FIDs were zero filled up to 64 k points

and Fourier transformed. Image reconstruction from these transforms was performed using filtered back projection methods.[25]

I. Magnet and gradient coils

Main magnet: The main magnetic field was generated by a Helmholtz pair (i.d. 30 cm) of water-cooled coils (GMW, Model 5451, Redwood City, CA) based on a fourth order homogeneous design. The field homogeneity was better than 10 ppm in the active volume of approximately 5 cm^3. The magnet was powered by a Danfysik 8000 (Danfysik, Jyllinge, Denmark) power supply.

Gradients: A shielded three axes, static gradient system (BFG-350/10; Resonance Research Inc., Billerica, MA) was incorporated into the main magnet to facilitate imaging experiments. Gradient coils (o.d. 30 cm, i.d. 10 cm, length 35 cm) were powered by an HP66000 unipolar power supply (Hewlett Packard, Palo Alto, CA) at 14-bit resolution. Data from test experiments indicated that at a current of 10 A, the strengths of individual gradients were 5.3, 5.4, and 7.5 G/cm in the X, Y, and Z directions, respectively. The coils were cooled by forced room air. The maximum gradients which could be generated were 5 G/cm over a 5 cm diameter sphere with a uniformity of better than 1%. The gradient vector magnitude and direction were controlled by the computer through an IEEE interface with a gradient settling time of less than 0.1 s. Using spin probes with narrow EPR linewidths (150 mG) and a field gradient of 1 G/cm (which corresponds to 2.8 MHz/cm), we can in principle resolve two points separated by 2 mm corresponding to a resonance shift of 200 mG. Furthermore, with a gradient of just 1 G/cm, objects of size up to 5 cm^3 can be imaged with about 2 mm resolution. The field of view in frequency is approximately 12 MHz, almost close to the power spectral width of a 75 ns pulse and a resonator with a Q of 25. Image quality can be further improved by using pulses of 35 ns duration at a higher power level which will irradiate the system more uniformly and still provide adequate signal.

J. Host computer

A Silicon Graphics IRIS 4D computer was used for spectrometer control, data collection, and processing. Spectrometer modules were interfaced to the computer by GPIB (IEEE 488) and RS 232C connections. The application programs were written in Matlab (The Math Works, Inc., Natick, MA). The back projection algorithm was written in C language.

K. Spin probes

The desired characteristics of spin probes suitable for rf FT EPR spectroscopy and imaging are that the time-domain signal lasts beyond the spectrometer dead time of 450 ns; i.e., the spin probes should have narrow single lines. An example of spin probes having such characteristics is the charge-transfer compound, N-methylpyridinium tetracyanoquinodimethane (NMP-TCNQ).[26]

III. RESULTS

Detection of the FIDs of solid NMP-TCNQ after pulsed excitation at 300 MHz resonant frequency was carried out. NMP-TCNQ contains a paramagnetic center ($S=1/2$) exhibiting a single line with an oxygen-insensitive linewidth of 0.18 G. An overcoupled resonator that had a diameter of 25 mm and a height of 25 mm containing 11 parallel loops 2.5 mm apart, was used for detection and imaging. These dimensions were adequate to accommodate an experimental animal, such as a mouse, for imaging studies. The loaded Q of the coil was maintained at 25. Pulses of 70 ns duration (283 Vpp), were used for excitation. The spectral bandwidth afforded by such pulses was at least 12 MHz. Dead times typically ranged between 300 and 450 ns after the pulse. Data acquisition was initiated 250 ns after the trailing edge of the pulse, during the resonator dead time to allow the summer to settle. In the digitized wave form, the initial 250 points, corresponding to 250 ns were discarded before data processing. With the rf phase set at 0°, a set of 80 000 FIDs, 4 k points each, were collected and averaged. After downloading the data to the host computer, the rf phase was changed to 180° and another set of 80 000 FIDs was collected. The average of the phase changed FIDs was subtracted from the average of the previous group of FIDs to remove systematic noise. The FIDs were zero filled and Fourier transformed.

Figure 4(A) shows the schematic of the phantom sample containing four tubes filled with about 4 mg each of the solid NMP-TCNQ. The four tubes were placed in the resonator and collinear about the X axis and having the same center of gravity as the resonator. The separation between the extreme tubes is approximately 20 mm, while the separation between the outer and the inner tubes is approximately 10 mm (center to center). The two inner tubes are separated by the wall thicknesses of the tubes (approximately 0.25 mm). The dotted lines represent the windings of the resonator coils. Figure 4(B) shows a typical FID obtained when a field gradient of 1.1 G/cm was applied along the X axis. The interferogram shows the frequency encoding of the four tubes containing the spin probe in the phantom sample along the X axis. The corresponding absorption spectrum was obtained by Fourier transformation shown in Fig. 4(C) exhibiting clearly resolved four absorption peaks corresponding to the individual tubes. For spatial encoding of the spins, the gradient was rotated in the plane perpendicular to the imaging plane in steps of 5°, and 36 projections were acquired using a gradient strength of 1.1 G/cm. FIDs corresponding to each projection were zero filled up to 64 k points and filtered in time domain using a line-narrowing exponential filter for resolution enhancement and subjected to Fourier transformation. For image reconstruction, spectra were subsampled to 127 points, filtered by a Shepp–Logan filter, and back projected to obtain the two-dimensional image. In a typical two-dimensional imaging experiment, the time taken for the data collection was approximately 2 min. The resulting two-dimensional projections in the three orthogonal planes were obtained from such experiments and are shown in Figs. 5(A)–5(C). The slightly differing resolution and magnifica-

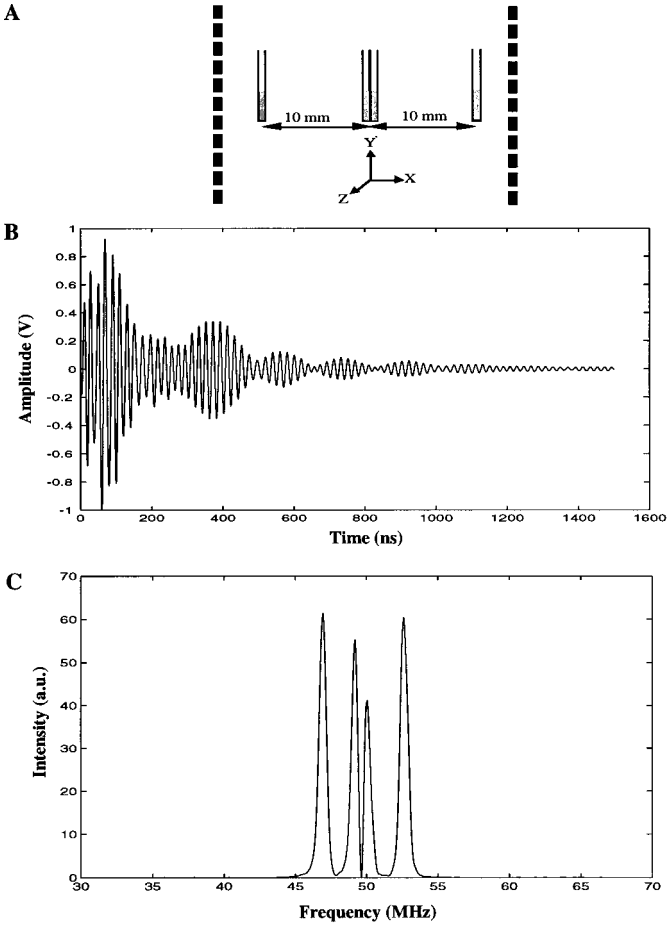

FIG. 4. (A) Schematic of the four-tube phantom used for imaging. The four tubes were filled with approximately 4 mg of NMP-TCNQ each in capillary tubes (1 mm i.d.). The tubes are colinearly arranged along the X axis with their axes parallel to Y axis. The outer tubes are about 10 mm from the center while the inner tubes are placed next to each other separated by their wall thickness. The sample occupied a column height of approximately 4 mm. No efforts were made to load the four tubes identically with the spin probe. (B) A typical FID sampled at 1 GS/s, containing the first 1500 points of a 4000 point data set, obtained from the four tube phantom under a gradient of 1.1 G/cm along the X axis. A total of 160 000 individual FIDs of 4 k points were averaged. (C) The absorption spectrum obtained by FT of the FID in (B).

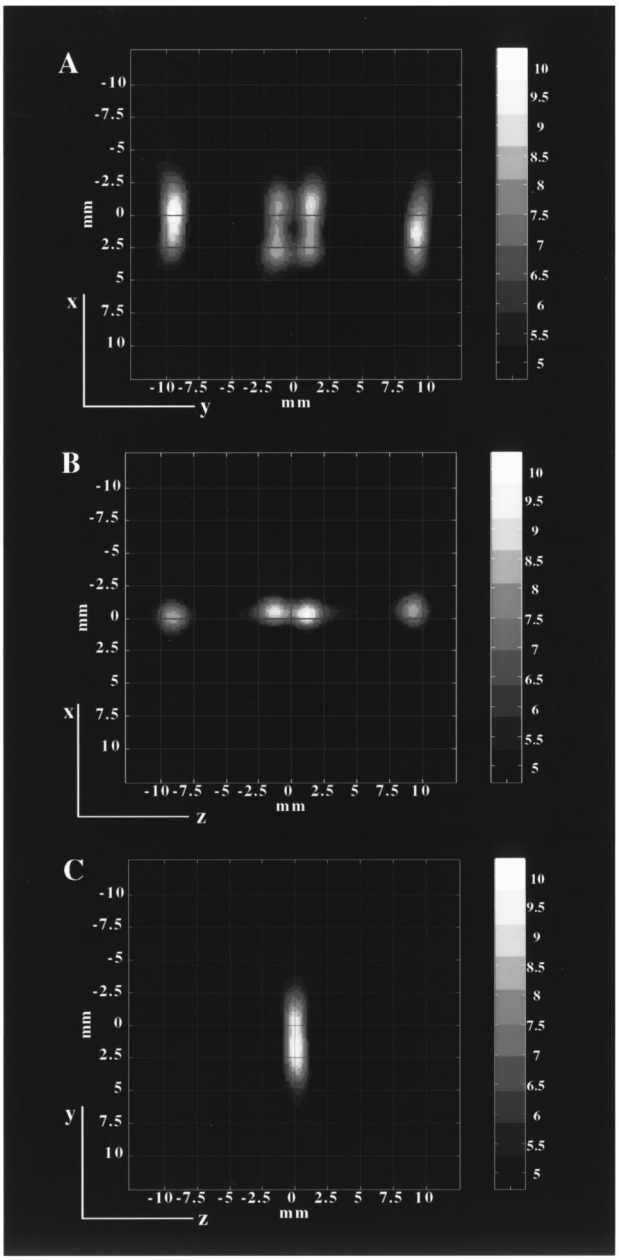

FIG. 5. Two-dimensional images of the four-tube phantom containing NMP-TCNQ described in Fig. 4(A). Two-dimensional projection of the EPR image in the (A) XY, (B) XZ, and (C) YZ planes. In all these experiments a linear gradient of 1.1 G/cm was used. These are not cross sections from a single 3D image, but are 2D projections of the unpaired spin density about the three orthogonal axes X, Y, and Z.

tion seen on the figures are due to the fact that these are not orthogonal slices taken from a single 3D image, but are rather 2D projections of the unpaired spin densities about the three orthogonal axes derived from *three different* 2D experiments. Therefore the back projections are subject to some distortions depending upon the actual geometry and symmetry of the spin distribution. The field gradients have been verified to be uniform to an accuracy of better than 1% in a sphere of diameter 5 cm about the center of the magnet and center of gravity of the gradient coils. The three projections corresponded to the physical dimensions of the phantoms in spin density, physical separation, and orientation.

In separate experiments, we have verified that the presence of phosphate buffered saline (PBS) does not adversely affect the image quality (data not shown) indicating, that at best, minimal rf penetration problems are associated with obtaining spatial images of the spin probe in material equivalent to biologic tissue. Surface coil resonators were also used to test the feasibility of detecting spin probes in large and lossy objects and was found to give results that are similar to the ones obtained in NMR and will be potentially useful for topical studies.

IV. DISCUSSION

Although EPR, at a given field is more sensitive than NMR, the low concentration of endogenous free radicals in biological objects severely limits the SNR in *in vivo* objects. However, using nontoxic exogenous spin probes, it is possible to obtain anatomical detail by EPR imaging at radio frequencies.[4,6,9,10,23,31,32] In addition, by adding a spectral di-

mension to the spatial imaging methods, important physiologic information could be obtained as well.[4,10,11] This capability makes EPRI a potentially low-cost technique complementary to other imaging techniques such as MRI or PET, and aid in the identification of pathophysiological volumes in human objects noninvasively. For example, by spectral-spatial imaging, pO_2 values *in vivo* can be obtained. In addition, with the increasing sensitivity of EPRI at clinically relevant tissue oxygenation levels encountered in pathological conditions, EPRI may well find a unique place to detect and map hypoxic volumes.[27,28] Such measurements should provide valuable physiologic information with respect to the pO_2 status of tumor versus normal tissue. This information may help in devising more aggressive therapeutic regimens for patients with large hypoxic fractions in tumors.

EPRI has been implemented at *X* band, *L* band, and most recently at the radio frequency region to afford better tissue penetration while minimizing nonresonant absorption.[3,4] Most of these spectrometers reported so far operate in the frequency domain. However, at *X*-band frequency using pulsed excitation, Fourier EPR imaging was performed to obtain high resolution images of spin probes.[29,30] At lower frequencies and using cw EPR methods and exogenous spin probes, spatial as well as spectral-spatial imaging experiments provided valuable information on intact biologic objects, such as isolated viable organs and small laboratory animals. However, limitations in imaging with cw EPR were encountered because of motion resulting from heartbeat, respiration, etc. These problems had to be addressed with special gating approaches to avoid distortions in the image[31] as well as a constant infusion of the spin probe to maintain adequate signal for image reconstruction. Though EPRI experiments on viable biologic objects in time domain are minimally affected by physiological motions, such techniques have not been developed primarily because of lack of spin probes having sufficiently long spin-spin relaxation times to permit detection using existing technology. With the recently available spin probes possessing narrow single lines,[23,32] EPRI using pulsed excitation provides sensitivity, based on the Fellgett multichannel advantage inherent in the time domain data acquisition method.[13] The gain in sensitivity might at least equal that of cw techniques at the same frequency. Pulsed rf EPR imaging spectrometers have been reported for studying small volumes.[21–23] Using narrow line spin probes which are nontoxic and infusible, high resolution images of spin probe distribution in the tail circulatory anatomy in a murine model was obtained.[23] However, for more useful *in vivo* applications as in the case of MRI, capabilities to study the whole body of small experimental animals such as mice should be developed. With these capabilities, using methods established in MRI, physiologic information such as tissue oxygen status and redox status can be obtained with EPR imaging and infusible probes.

Though in principle similar to NMR imaging, the implementation of time-domain EPRI for *in vivo* applications requires developmental efforts in all aspects of the spectrometer, namely, the transmit arm, the receive arm, the resonator, and the data acquisition system. Narrow pulses with durations in the order of 10–80 ns have to be generated which contain at least several cycles of the resonant frequency for selectivity in excitation. The pulses should be amplified significantly, with minimal rise times associated with pulse amplification, to provide the necessary nutation of the spin systems in the resonator. The resonator should be able to accommodate the object under study in terms of physical dimension as well as spectral bandwidth. Additionally, the dead time should be minimal. The first stage amplifier should possess rapid recovery times, low noise, and high gain; all these are necessary to detect rapidly decaying signals of the electron spins. Moreover, to exploit the faster relaxation behavior of electron spins for signal enhancement, rapid digitization and averaging strategies have to be implemented.

In this study, the details of the spectrometer for *in vivo* operation to detect and image spin probes in a biologic object the size of a mouse are described which incorporate the above mentioned aspects in a modular manner. Narrow pulses of width ranging from 10 to 80 ns were generated by high-speed gates. The transmit power necessary to irradiate the sample housed in a resonator of 25 mm bore diameter and 25 mm height was obtained by coupling two power amplifiers, each of 100 W capacity. Since the resonator was of single coil design, the use of a transmit/receive diplexer was preferred over the circulator to avoid excessive insertion losses. The diplexer diodes had switching times less than 5 ns and provided an isolation of 25 dB between the transmitter and the receiver. This provided the necessary sensitivity in terms of excitation as well as the desired bandwidth for spectroscopic as well as imaging experiments. The first stage amplifier in the receive arm was designed to avoid overload and also facilitate fast recovery to detect and amplify the weak resonance signals. After further amplification and filtering, rapid digitizing and averaging provided adequate SNR in times much shorter than in the case of NMR. All aspects were implemented in the spectrometer to provide the necessary sensitivity to successfully detect EPR in time domain using pulsed excitation. Imaging experiments were performed using volume excitation methods in the presence of static gradients. Such methods have inherently more sensitivity than the slice selection methods using pulsed gradients that is routinely practiced in MRI, but require longer imaging times. Using static gradients, the images obtained from the 2D spatial imaging experiments of the phantoms containing the spin probes, indicate a resolution better than 0.2 mm with imaging times of less than 2 min and a good correlation with the physical dimensions of the phantom objects. The implementation of slice selection methods in EPRI becomes feasible with the development of gradient settling times in the order of the dead times of the resonator and further minimize imaging times. With the current version of the EPRI spectrometer, dead times in the order of 300–450 ns with loaded *Q* values of about 25 were noted for input powers of up to 200 W. Additional improvements in terms of diplexers with improved isolation, dynamic *Q* spoiling to increase the resonator sensitivity, digitizers with higher vertical resolution at the required speed should provide enhanced sensitivity for imaging applications. In addition, nontoxic spin probes with narrow linewidths of the order of 25–150 mG dependent on

oxygen are being used to image tissue oxygenation status using double resonance imaging techniques such as Overhauser enhanced MRI.[33,34] Such probes are optimal for time-domain EPR imaging as well, since their FIDs survive for sufficient times (1–5 μs) after the dead times.[23] Therefore, EPRI has the potential to become a diagnostic tool, not only for spatial imaging, but also to obtain valuable physiologic information noninvasively.

[1] P. A. Bottomley and E. R. Andrew, Phys. Med. Biol. **23**, 630 (1978).
[2] P. Roschmann, Med. Phys. **14**, 922 (1987).
[3] M. Grandolfo, P. Vecchia, and O. P. Gandhi, Bioelectromagnetics (N.Y.) **11**, 117 (1990).
[4] H. J. Halpern, C. Yu, M. Peric, E. Barth, D. J. Grdina, and B. A. Teicher, Proc. Natl. Acad. Sci. USA **91**, 13047 (1994).
[5] W. Froncisz and J. S. Hyde, J. Magn. Reson. **47**, 515 (1982).
[6] H. J. Halpern, D. P. Spencer, J. van Polen, M. K. Bowman, A. C. Nelson, E. M. Dowey, and B. A. Teicher, Rev. Sci. Instrum. **60**, 1040 (1989).
[7] Y. Miura, H. Utsumi, and A. Hamada, Biochem. Biophys. Res. Comm. **182**, 1108 (1992).
[8] T. Yoshimura, S. Fujii, H. Yokoyama, and H. Kamada, Chem. Lett. **4**, 309 (1995).
[9] M. Alecci, S. D. Penna, A. Sotgiu, L. Testa, and I. Vannucci, Rev. Sci. Instrum. **63**, 4263 (1992).
[10] P. Kuppusamy, M. Chzhan, K. Vij, M. Shteynbuk, D. J. Lefer, E. Giannella, and J. L. Zweier, Proc. Natl. Acad. Sci. USA **91**, 3388 (1994).
[11] K. J. Liu, P. Gast, M. Moussavi, S. W. Norby, M. Wu, and H. M. Swartz, Proc. Natl. Acad. Sci. USA **90**, 5438 (1993).
[12] J. L. Berliner and H. Fujii, Science **227**, 517 (1985).
[13] R. R. Ernst and W. A. Anderson, Rev. Sci. Instrum. **37**, 93 (1966).
[14] M. Huisjen and J. S. Hyde, Rev. Sci. Instrum. **45**, 669 (1974).
[15] P. W. Percival and J. S. Hyde, Rev. Sci. Instrum. **46**, 1522 (1975).
[16] J. P. Hornak and J. H. Freed, J. Magn. Reson. **67**, 501 (1986).
[17] R. W. Quine, G. R. Eaton, and S. S. Eaton, Rev. Sci. Instrum. **58**, 1709 (1987).
[18] M. K. Bowman, in *Modern Pulsed and Continuous Wave Electron Spin Resonance*, edited by L. Kevan and M. K. Bowman (Wiley, New York, 1990), pp. 1–42.
[19] B. E. Sturgeon and R. D. Britt, Rev. Sci. Instrum. **63**, 2187 (1992).
[20] S. Pfenninger, W. Froncisz, J. Forrer, J. Luglio, and J. S. Hyde, Rev. Sci. Instrum. **68**, 4857 (1995).
[21] J. Bourg, M. C. Krishna, J. B. Mitchell, R. G. Tschudin, T. J. Pohida, W. S. Friauf, P. D. Smith, J. Metcalfe, F. Harrington, and S. Subramanian, J. Magn. Reson. **102**, 112 (1993).
[22] T. J. Pohida, H. A. Frederickson, R. G. Tschudin, J. F. Fessler, M. C. Krishna, J. Bourg, F. Harrington, and S. Subramanian, Rev. Sci. Instrum. **65**, 2500 (1994).
[23] R. Murugesan, J. A. Cook, N. Devasahayam, M. Afeworki, S. Subramanian, R. Tschudin, J. H. A. Larsen, J. B. Mitchell, A. Russo, and M. C. Krishna, Magn. Reson. Med. **38**, 409 (1997).
[24] F. J. Harris, Proc. IEEE **66**, 51 (1978).
[25] R. K. Woods, W. B. Hyslop, R. B. Marr, and P. C. Lauterbur, in *EPR Imaging and In Vivo EPR*, edited by G. R. Eaton, S. S. Eaton, and K. Ohno (CRC, Boca Raton, FL, 1991), pp. 91–118.
[26] P. B. Ayscough, in *Electron Spin Resonance in Chemistry* (Butler and Tanner, London, 1967), pp. 415–422.
[27] U. Ewert, R. H. Crepeau, C. R. Dunnam, D. Xu, S. Lee, and J. H. Freed, Chem. Phys. Lett. **184**, 25 (1991).
[28] D. J. Sloop, H. L. Yu, and T. S. Lin, Chem. Phys. Lett. **124**, 456 (1986).
[29] P. Kuppusamy, M. Chzhan, P. Wang, and J. L. Zweier, Magn. Reson. Med. **35**, 323 (1996).
[30] P. Kuppusamy, P. Wang, M. Chzhan, and J. L. Zweier, Magn. Reson. Med. **37**, 479 (1997).
[31] H. B. Stone, J. M. Brown, T. L. Phillips, and R. M. Sutherland, Radiat. Sci. **136**, 422 (1993).
[32] G. R. Eaton and S. S. Eaton, Bull. Magn. Reson. **10**, 22 (1989).
[33] K. Golman, I. Leunbach, J. H. A. Larsen, G. Ehnholm, L. G. Wistrand, J. S. Petersson, and S. Vahasalo, Acta Radiol. **39**, 10 (1998).
[34] J. H. A. Larsen, I. Laursen, I. Leunbach, G. Ehnholm, L. G. Wistrand, J. S. Petersson, and K. Golman J. Magn. Reson. (in press).